Journal of Biomolecular NMR (2006) 34: 197–202
DOI 10.1007/s10858-006-0018-6

NMR structure note

Solution structure of the FK506-binding domain of human FKBP38

Mitcheell Maestre-Martínez, Frank Edlich, Franziska Jarczowski, Matthias Weiwad, Gunter Fischer & Christian Lücke*
Max Planck Research Unit for Enzymology of Protein Folding, D-06120 Halle a.d. Saale, Weinbergweg 22, Germany

Received 7 December 2005; Accepted 20 January 2006

Key words: calcineurin, calmodulin, immunophilins, immunosuppression, PPIases

Abbreviations: Bad – Bcl-2 antagonist of cell death; Bcl-2 – B-cell leukemia/lymphoma 2; CaM – calmodulin; CaN – calcineurin; hFKBP38D – FK506-binding domain of human FKBP38; HSQC – heteronuclear single-quantum correlation; HTQC – heteronuclear triple-quantum correlation; NF-AT – nuclear factor of activated T cell; NOESY – nuclear Overhauser enhancement spectroscopy; PPIase – peptidyl prolyl *cis*/*trans* isomerase; RMSD – root-mean-square deviation; TOCSY – total correlation spectroscopy; TPR – tetratricopeptide repeat

Biological context

FKBP38 belongs to the peptidyl prolyl *cis*/*trans* isomerase (PPIase) family of FK506-binding proteins (FKBPs) (Fischer, 1994). The enzyme class of PPIases assists other proteins in the folding process by catalyzing the interconversion between the *cis* and *trans* conformation of peptide bonds preceding proline residues in the polypeptide chain. PPIases thus contribute to *de novo* protein folding and conformational rearrangements in native proteins (Fischer and Aumüller, 2003). Hence, PPIases play a role in signal transduction processes by controlling the activity of their substrate proteins.

Beyond their enzymatic activity, FKBPs are known to be involved in immunosuppression by forming tight complexes with the low-molecular weight compound FK506. In particular the interaction between the FK506/FKBP12 complex and the protein phosphatase calcineurin (PP2B or more commonly abbreviated as CaN) has been reported to mediate the immunosuppressive properties of FK506 (Liu et al., 1991). The resulting FKBP12/FK506/CaN complex prevents T-cell proliferation by inhibiting the protein phosphatase activity of calcineurin and consequently NF-AT signalling. Therefore FKBPs are also referred to as immunophilins.

Recently, FKBP38 was reported as an inherent calcineurin inhibitor, suggesting that it is the only immunophilin that interferes with the CaN/NF-AT pathway in the absence of its immunosuppressive ligand (Shirane and Nakayama, 2003). However, there is clear evidence that FKBP38 cannot inhibit CaN in the absence of FK506, rendering impossible its role as endogeneous calcineurin inhibitor (Kang et al., 2005; Weiwad et al., 2005).

Nevertheless, FKBP38 possesses unique properties among the human FKBPs in that its enzymatic activity was found to be CaM/Ca^{2+}-dependent (Edlich et al., 2005). Hence, FKBP38 is the only human FKBP that is regulated by a secondary messenger, implying different structural features of its FKBP domain compared to those of constitutively active FKBPs. Previous work of our group indicated that formation of the FKBP38/CaM/Ca^{2+} complex induces structural changes in

*To whom correspondence should be addressed. E-mail: luecke@enzyme-halle.mpg.de

the tertiary structure of FKBP38. This enzymatically active form of FKBP38 interacts with Bcl-2, which is known to be a key player in the control of apoptosis. The Bcl-2/FKBP38/CaM/Ca^{2+} complex interferes with the binding of Bcl-2 to its cellular targets, such as CaN or Bad. Thus, the active form of FKBP38 participates in apoptosis control by inhibition of the anti-apoptotic Bcl-2 function. The formation of the Bcl-2/FKBP38/CaM/Ca^{2+} complex, however, can be prevented by application of specific FKBP38 inhibitors. In fact, the inhibition of FKBP38 by active site-directed ligands or the reduction of cellular FKBP38 levels by FKBP38 RNAi in neuroblastoma cells resulted in a prevention of apoptosis that is induced by either etoposide, daunorubicin, camptothecin or ionomycin. This result strongly suggests a role of FKBP38 in the regulation of apoptosis in neuronal systems.

The solution of the three-dimensional FKBP38 structure will contribute to understanding the molecular basis of its biological function(s) and the mechanism(s) by which its enzymatic activity is controlled. In this context, the N-terminal FKBP domain of human FKBP38 is of special interest. FKBP domains typically adopt a "half β-barrel" fold, which (i) consists of an antiparallel β-sheet that wraps around a central α-helix and (ii) encloses the active site (Van Duyne et al., 1991). In the sequence of FKBP38, the FKBP domain is followed by a tetratricopeptide repeat (TPR) domain. The structural arrangement of FKBP38 is therefore similar to FKBP51 and FKBP52 (Li et al., 2003; Sinars et al., 2003), yet contains only a single FKBP domain. The TPR domain most likely contains three TPR motifs, each consisting of two α-helices. The C-terminal end of the TPR domain in FKBP38 contains a putative CaM-binding site. The FKBP38 sequence is completed by a membrane anchor that is also unique among the human FKBPs. The determination of the N-terminal FKBP domain structure is only the first step in elucidating the entire FKBP38 molecule and its biological features.

Methods and results

Cloning, expression and purification

Based on preliminary NMR experiments with a longer construct, the first 34 residues of the FKBP38 N-terminus appeared to be unstructured. Therefore, we decided to clone only the fragment comprising residues 35–153. To obtain recombinant human $FKBP38^{35\text{-}153}$, the nucleotide sequence was amplified by PCR with the following primers: 5′-GACTTCATGAGAAGAGTGGCT GGACATTCTG-3′ and 5′-GACTAAGCTTTCA CTCCAGGTCAGGCCCG-3′. The PCR product was subcloned into a pSTBlue-1 vector (Novagen, Madison, WI, U.S.A.), digested with *Bsp*HI/*Hin*dIII, ligated into a pET28a vector, and finally transformed into BL21(DE3) Rosetta cells (Novagen, Madison, WI, U.S.A.). The resulting construct (hFKBP38D), which included two additional residues Met33 and Arg34 at the N-terminal end as cloning artifacts, was verified by restriction analysis and DNA sequencing.

Protein expression of hFKBP38D in LB medium at 37 °C was induced by adding isopropyl-β-D-thiogalactoside to a final concentration of 1 mM and subsequent incubation for another 4 h. For ^{15}N-labelling, the cells were grown and expressed in a fully ^{15}N-enriched "rich growth OD2" medium (Silantes GmbH, München, Germany). Next, cells were harvested by centrifugation for 15 min at 4 °C and 5000 × *g*. The bacterial pellet from a 6 l culture was resuspended in 200 ml lysis buffer (10 mM MES pH 6.0, 150 mM NaCl) and cracked in a French press. The supernatant was centrifuged for 45 min at 4 °C and 100,000 × *g*.

The soluble cell lysate was applied to a Fractogel EMD DEAE-650 column (Merck, Whitehouse Station, NJ, U.S.A.) equilibrated with 10 mM MES buffer (pH 6.0, 150 mM NaCl). The protein was eluted from the DEAE-650 column with 1 M NaCl and the fractions were analyzed on a 15% (w/v) SDS-PAGE gel stained with Coomassie blue. The fractions containing hFKBP38D were dialyzed against 10 mM HEPES buffer (pH 7.8, 1.5 mM $MgCl_2$, 150 mM KCl) and loaded on a HiLoad 16/60 Superdex 200 pg column (GE Healthcare, Waukesha, WI, U.S.A.) according to the recommendations of the supplier. The protein fractions were analyzed on a 15% (w/v) SDS-PAGE gel stained with Coomassie blue. hFKBP38D was subsequently analyzed by MALDI-TOF mass spectrometry and N-terminal protein sequencing, thereby confirming the identity of the protein.

NMR measurements

The NMR samples were prepared by dissolving either non-labelled or ^{15}N-enriched hFKBP38D (1.3–1.4 mM) in 20 mM sodium phosphate buffer (pH 6.7, 0.05% sodium azide, 5% D_2O). NMR data were collected with DRX500 and Avance-700 spectrometers (Bruker, Rheinstetten, Germany), operating at 500.13 and 700.13 MHz proton resonance frequencies, respectively, and both equipped with 5 mm inverse triple-resonance (^{1}H/^{13}C/^{15}N) probes that have XYZ-gradient capability. Homonuclear two-dimensional (2D) spectra (TOCSY and NOESY) as well as ^{15}N-edited multidimensional spectra were acquired; the latter included 2D HSQC, 2D HTQC, 3D TOCSY-HSQC and 3D NOESY-HSQC. The TOCSY experiments were performed with spin-lock times of either 80 ms or 6 ms (to obtain COSY-type information with less spectral overlap). For the NOESY experiments, a mixing time (τ_m) of 150 ms was used. In the homonuclear one- and two-dimensional ^{1}H experiments, the water signal was suppressed by selective presaturation during the relaxation delay, with the carrier placed in the centre of the spectrum on the water resonance. All heteronuclear experiments made use of pulsed field gradients for coherence selection and artifact suppression, and utilized gradient sensitivity enhancement schemes wherever appropriate (Muhandiram and Kay, 1994). All NMR experiments were acquired at 25 °C in a phase-sensitive mode. Quadrature detection in the indirectly detected dimensions was obtained either by the States-TPPI or by the echo/anti-echo method. The chemical shifts were referenced to external 2,2-dimethyl-2-silapentane-5-sulfonate (Cambridge Isotope Laboratories, Andover, MA, USA) in order to ensure consistency among all spectra (Wishart et al., 1995).

All spectra were processed and analyzed on a Silicon Graphics O2 workstation using the XWINNMR 3.5 software package (Bruker, Rheinstetten, Germany). A 90° phase-shifted squared sine-bell function was used for apodization in all dimensions. Polynomial base-line correction was applied to the processed spectra wherever necessary. Peak picking and data analysis of the transformed spectra were performed using the AURELIA 2.5.9 (Bruker, Rheinstetten, Germany) and FELIX 2000 (Accelrys Inc., San Diego, CA, U.S.A.) software packages.

Structure determination

The sequence-specific ^{1}H and ^{15}N assignments were determined through NOE connectivities according to the classical assignment strategy (Wüthrich, 1986). The resonance assignment of hFKBP38D is basically complete, except for the backbone amide groups of the two cloning artifacts Met33 and Arg34, and has been deposited at the BioMagResBank database under accession number BMRB-6902. Pro129 was found to be in a *cis* conformation; all other proline residues are *trans* forms, as indicated by the observation of strong NOE connectivities between the proline Cδ protons and the Hα of the corresponding preceding residues (Wüthrich, 1986).

The NOE-derived distance restraints were determined from homonuclear 2D NOESY and 3D ^{15}N-edited NOESY-HSQC spectra (Figure 1). Automated assignments of the NOEs, based on chemical shifts only, were obtained with the program *nmr2st* (Pristovšek et al., 2000). An internal calibration, based on the intensities of characteristic intra- and inter-strand NOEs within the β-sheet structure as well as sequential and medium-range NOEs within the α-helix, was used to set the upper distance limits. The integrated peak volumes were converted into approximate interproton distances by normalizing against the calibrated volumes. The upper distance bounds were subsequently set to different categories of 2.5, 3.5, 4.5 and 6.0 Å.

The structures were calculated on a Silicon Graphics O2 workstation with the program DYANA 1.5 (Güntert et al., 1997), which uses a simulated annealing algorithm combined with torsion angle dynamics. Starting *ab initio*, 100 conformers were calculated in 8000 annealing steps each. An iterative strategy was used for the structure refinement; in each round of structure refinement, the newly computed NMR structures were employed to (i) assign ambiguous NOE cross-peaks, (ii) correct erroneous assignments, and (iii) loosen the NOE distance bounds if spectral overlap was deduced.

Stereospecific assignments were obtained for nearly all prochiral amide (6), isopropyl (26) and methylene (76) groups with the program GLOMSA (Güntert et al., 1991). Pseudo-atom correction for magnetically equivalent protons was applied as proposed by Wüthrich et al. (1983). No hydrogen

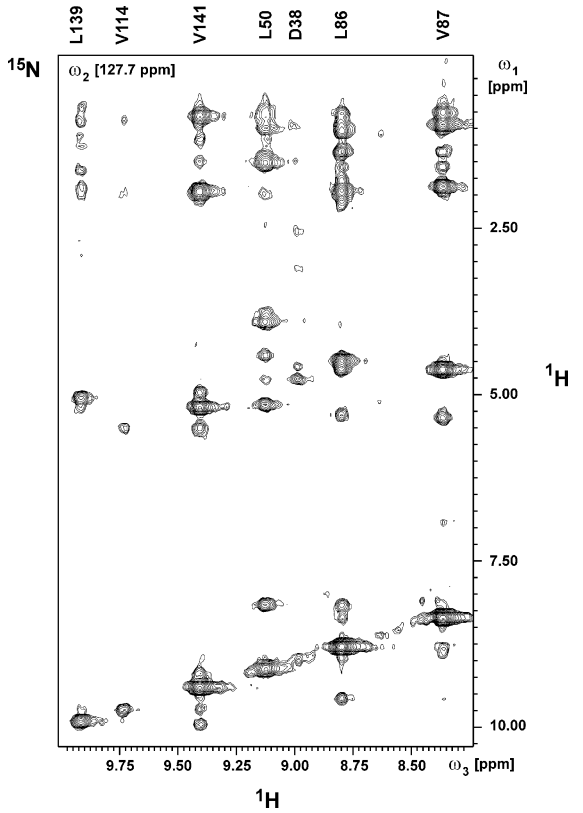

Figure 1. $^{1}H/^{1}H$ plane at 127.7 ppm ^{15}N chemical shift from the 3D NOESY-HSQC spectrum of hFKBP38D (500.13 MHz proton resonance frequency; 150 ms mixing time). Residues with amide group resonances located either in this particular or in adjacent planes are assigned above the spectrum.

bond constraints were used in the structure calculation.

In the last run of calculations the structures were computed using 1585 meaningful distance restraints, obtained out of a total of 2191 NOE assignments. Subsequent energy minimization in the presence of the NOE-derived distance restraints, carried out with the DISCOVER module of the INSIGHT 2000 software package (Accelrys, San Diego, CA, U.S.A.), was performed on the 20 best DYANA conformers. The consistent valence force field (Dauber-Osguthorpe et al., 1988) was used with a dielectric constant equal to r (distance in Å). A force constant of 20 kcal $Å^{-2}$ mol^{-1} was applied in the NOE restraint term. The 20 final selected hFKBP38D conformers were analyzed with PROCHECK-NMR (Laskowski et al., 1996); the structural statistics are listed in Table 1.

Table 1. Structural statistics of the final 20 energy-minimized hFKBP38D conformers

NOE-derived distance restraints	1585
Intraresidual ($i=j$)	288
Sequential ($\mid i-j\mid=1$)	521
Medium-range ($1 < \mid i-j\mid \leq 4$)	194
Long-range ($\mid i-j\mid > 4$)	582
Total number of restraint violations >0.3 Å	0
Total number of restraint violations >0.2 Å	6
Maximal restraint violation (Å)	0.23
Ramachandran plot (%)	
Most favoured regions	69.8
Additionally allowed regions	25.5
Generously allowed regions	2.7
Disallowed regions	2.0
Backbone atom[a] RMSD (Å)	
Residues 36–149	1.73 ± 0.22
Residues 36–117, 136–149	1.48 ± 0.18
Secondary structure elements	1.08 ± 0.13
Heavy atom RMSD (Å)	
Residues 36–149	2.25 ± 0.23
Residues 36–117, 136–149	1.99 ± 0.22
Secondary structure elements	1.77 ± 0.25

[a]N, C^{α}, C′ and O.

Structural features of hFKBP38D

The solution structure of hFKBP38D was determined based on 1585 NOE-derived distance restraints. The atomic coordinates have been deposited in the RCSB database under accession number PDB ID 2F2D. Figure 2a shows a superposition of the final 20 energy-minimized hFKBP38D conformers. The NOE connectivity pattern between the backbone protons was used to determine the secondary structure elements of the protein. A large number of strong sequential $d_{\alpha N}(i, i+1)$ NOE connectivities indicated predominantly β-strand elements. Additional interstrand NOEs revealed an antiparallel β-sheet structure consisting of 6 β-strands: Leu37-Asp38 (βA), Leu45-Thr49 (βB), Gln64-Leu74 (βC), Thr78-Leu90 (βD), Glu110-Asp117 (βE) and Ala136-Asp148 (βF). The fourth β-strand βD, however, is interrupted by two bulges at residues Val80 and Pro84; in addition, β-strand βF shows a bulge at residue Lys144. Furthermore, based on a series of strong sequential $d_{NN}(i, i+1)$, weaker

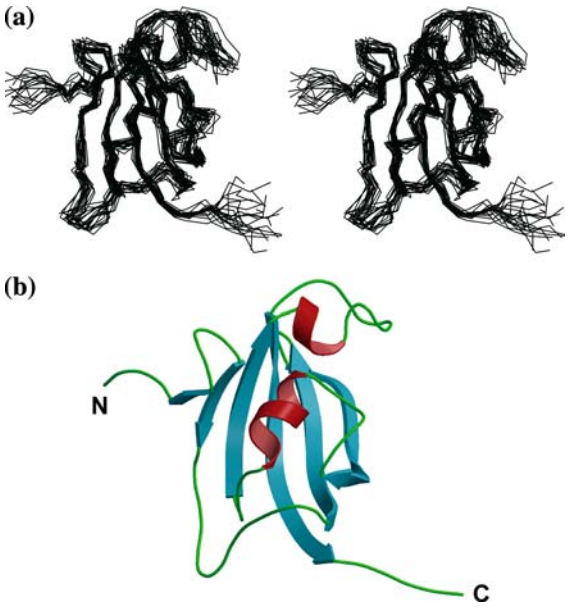

Figure 2. Representation of the hFKBP38D structure. (a) Stereo view showing the C^{α} traces of the 20 selected hFKBP38D conformers. (b) Ribbon diagram displaying the secondary structure elements of a single hFKBP38D conformer. The helical segments are colored in red, while β-strands are represented as blue arrows.

$d_{\alpha N}(i, i+1)$, as well as a dense network of medium-range $d_{NN}(i, i+2)$, $d_{\alpha N}(i, i+2)$, $d_{\alpha N}(i, i+3)$, $d_{\alpha\beta}(i, i+3)$ and $d_{\alpha N}(i, i+4)$ connectivities, an α-helix element spanning residues Gln97-Pro104 has been identified between β-strands βD and βE, with a slight kink at residue Val103. Another helical loop was found in the segment Ser118-Tyr122.

The overall structure of the 20 energy-minimized hFKBP38D conformers shows a backbone RMSD for the non-terminal residues (Trp36-Gly149) of 1.73 ± 0.22 Å and only few violations of the experimental constraints (Table 1). A six-stranded antiparallel β-sheet with a $+1, +3, +1, -3, +1$ topology curves around the central helix, thus forming a so-called "half β-barrel". Excluding the large Ser118-Ala135 loop, which covers the proposed FK506 binding pocket and shows a fairly high conformational variability, the RMSD of the backbone structure drops down to 1.48 ± 0.18 Å; excluding all loops structures, the backbone RMSD of just the secondary structure elements (one α-helix and six β-strands) decreases further to 1.08 ± 0.13 Å. Analysis of the backbone dihedral angles φ and ψ furthermore showed that 98% of all non-glycine/non-proline residues in hFKBP38D fall within the allowed regions of conformational space (Table 1).

Discussion and conclusions

The overall structure of apo hFKBP38D (Figure 2b) resembles the typical fold of FKBP domains, although this particular domain exhibits no PPIase activity and is not able to bind the low-molecular weight inhibitor FK506 in the absence of CaM. In comparison to the immunosuppressive FKBP12/FK506 complex (PDB ID code 1FKJ), the main structural difference is observed in β-strand βD between hFKBP38D residues Glu83 and Leu86 (see Figure 3); otherwise, the average backbone RMSD of 1.70 ± 0.19 Å between the X-ray structure of FKBP12 and the 20 hFKBP38D conformers (i.e., segments Leu45-Gly53, Gly56-Gly77, Val95-Thr115 and Ala136-Leu143) is comparable to the value obtained for the NMR ensemble itself (see Table 1).

In the case of hFKBP38D, β-strand βD is interrupted by only a small bulge affecting the positions of residues Pro84 and Glu85, whereas FKBP12 exhibits a larger loop (Arg40 – Pro45) with 4 additional residues. Consequently, the side-chain of Glu83 in hFKBP38D takes on a different orientation than the corresponding Ser39 side-chain in FKBP12, thereby extending into the putative FK506-binding site. Secondly, residue His87 near the entry portal to the FK506-binding site in FKBP12 is replaced by the larger side-chain of Arg127 in hFKBP38D, which shows a high degree of conformational variability in the 20 conformers of the hFKBP38D solution structure (Figure 3). Hence, the Arg127 side-chain, which reaches into the putative binding pocket in 80% of the conformers, could block the access to the ligand binding site. Moreover, Arg127 apparently can form salt bridge contacts inside the binding pocket with Glu83 and Asp94 (either separately or simultaneously), as observed in several of the NMR conformers; these salt bridge interactions (centroid distances between the guanidinium and carboxylate groups < 4 Å) might stabilize or possibly even constrict the entry portal region of hFKBP38D in contrast to FKBP12, and could thus be the molecular basis for the lack of PPIase activity and ligand binding.

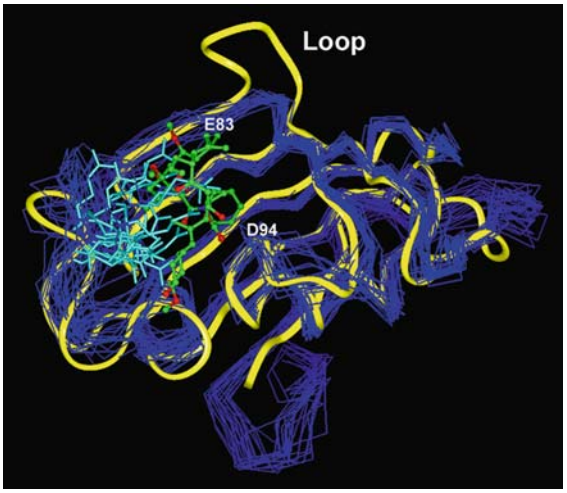

Figure 3. Superposition of the 20 selected hFKBP38D conformers (represented as C^{α} traces in blue) with the FKBP12/FK506 complex (yellow ribbon with ligand as ball-and-stick model; PDB ID code 1FKJ). The additional loop Arg40 – Pro45 in FKBP12 is labelled. Also marked are the backbone positions of residues Glu83 and Asp94 in hFKBP38D, which are possible salt bridge partners of Arg127. The Arg127 side-chains of the hFKBP38D conformers, which partially overlap with the FK506 ligand, are highlighted in cyan.

At this point, it is not clear exactly how hFKBP38D is activated by the presence of CaM. It appears highly unlikely, however, that hFKBP38D alone can mimick the CaN inhibitor FKBP12/FK506, since the only significant divergence in the backbone fold pertains to the above-mentioned bulge in β-strand βD. A comparison of those FKBP12 residues, which are located in the portal region next to the FK506 ligand, with the corresponding hFKBP38D residues also showed no other side-chains, except for Arg127, that would overlap with the volume of the bound FK506 ligand, thus providing structural background for the observations that FKBP38 cannot bind CaN in the absence of FK506 (Kang et al., 2005; Weiwad et al., 2005). Moreover, the amino acid replacements around the portal region (i.e., hFKBP38D segments Val80-Phe88, Gly91-Ile96 and Tyr120-Ile131) indicate a clear change in the net charge from +2 (or +3 if His87 is in the protonated state) in FKBP12 to −4 in hFKBP38D. This charge difference of 6 (or 7) units in the surface potentials around the entry portal of the two related FKBP domains may be important for substrate discrimination and could therefore be an explanation for their distinct functional behaviours.

Acknowledgements

The 700 MHz NMR spectra were collected externally at the Institute for Analytic Chemistry (University of Leipzig). The authors would like to thank Beate Rappsilber, Suzanne Roß and Monika Seidel (Max Planck Research Unit for Enzymology of Protein Folding) for technical assistance.

References

Dauber-Osguthorpe, P., Roberts, V.A., Osguthorpe, D.J., Wolff, D.J., Genest, M. and Hagler, A.T. (1988) *Proteins* **4**, 31–47.

Edlich, F., Weiwad, M., Erdmann, F., Fanghänel, J., Jarczowski, F., Rahfeld, J.U. and Fischer, G. (2005) *EMBO J.* **24**, 2688–2699.

Fischer, G. (1994) *Angew. Chem. Int. Ed.*, **33**, 1415–1436.

Fischer, G. and Aumüller, T. (2003) *Rev. Physiol. Biochem. Pharmacol.* **148**, 105–150.

Güntert, P., Braun, W. and Wüthrich, K. (1991) *J. Mol. Biol.* **217**, 517–530.

Güntert, P., Mumenthaler, C. and Wüthrich, K. (1997) *J. Mol. Biol.* **273**, 283–298.

Kang, C.B., Tai, J., Chia, J. and Yoon, H.S. (2005) *FEBS Lett.* **579**, 1469–1476.

Laskowski, R.A., Rullmann, J.A., MacArthur, M.W., Kaptein, R. and Thornton, J.M. (1996) *J. Biomol. NMR* **8**, 477–486.

Li, P.Y., Ding, Y., Wu, B.L., Shu, C.L., Shen, B.F. and Rao, Z.H. (2003) *Acta Crystallogr. Sect. D: Biol. Crystallogr.*, **59**, 16–22.

Liu, J., Farmer, J.D. Jr., Lane, W.S., Friedman, J., Weissman, I. and Schreiber, S.L. (1991) *Cell* **66**, 807–815.

Muhandiram, D.R. and Kay, L.E. (1994) *J. Magn. Reson. Ser. B*, **103**, 203–216.

Pristovšek, P., Lücke, C., Reincke, B., Ludwig, B. and Rüterjans, H. (2000) *Eur. J. Biochem.* **267**, 4205–4212.

Shirane, M. and Nakayama, K.I. (2003) *Nat. Cell Biol.* **5**, 28–37.

Sinars, C.R., Cheung-Flynn, J., Rimerman, R.A., Scammell, J.G., Smith, D.F. and Clardy, J. (2003) *Proc. Natl. Acad. Sci. U.S.A.* **100**, 868–873.

Van Duyne, G.D., Standaert, R.F., Karplus, P.A., Schreiber, S.L. and Clardy, J. (1991) *Science* **252**, 839–842.

Weiwad, M., Edlich, F., Erdmann, F., Jarczowski, F., Kilka, S., Dorn, M., Pechstein, A. and Fischer, G. (2005) *FEBS Lett.* **579**, 1591–1596.

Wishart, D.S., Bigam, C.G., Yao, J., Abildgaard, F., Dyson, H.J., Oldfield, E., Markley, J.L. and Sykes, B.D. (1995) *J. Biomol. NMR* **6**, 135–140.

Wüthrich, K., Billeter, M. and Braun, W. (1983) *J. Mol. Biol.* **169**, 949–961.

Wüthrich K. (1986) *NMR of Proteins and Nucleic Acids*. Wiley, New York, NY.